AFRL-MN-EG-TP-2006-7421

AN INVESTIGATION OF A DYNAMIC SENSOR MOTION STRATEGY

Nathan P. Yerrick
David E. Jeffcoat
Air Force Research Laboratory
Munitions Directorate
AFRL/MNGN
Eglin AFB, FL 32542-6810

Abhishek Tiwari
Engineer and Applied Sciences
California Institute of Technology
1200 California Blvd.
Pasadena, CA 91125

DECEMBER 2006

CONFERENCE PAPER

AIR FORCE RESEARCH LABORATORY, MUNITIONS DIRECTORATE

■ **Air Force Materiel Command** ■ **United States Air Force** ■ **Eglin Air Force Base**

REPORT DOCUMENTATION PAGE

The public reporting burden for this collection of information is estimated to average 1 hour per response, including the time for reviewing instructions, searching existing data sources, gathering and maintaining the data needed, and completing and reviewing the collection of information. Send comments regarding this burden estimate or any other aspect of this collection of information, including suggestions for reducing the burden, to Department of Defense, Washington Headquarters Services, Directorate for Information Operations and Reports (0704-0188), 1215 Jefferson Davis Highway, Suite 1204, Arlington, VA 22202-4302. Respondents should be aware that notwithstanding any other provision of law, no person shall be subject to any penalty for failing to comply with a collection of information if it does not display a currently valid OMB control number.
PLEASE DO NOT RETURN YOUR FORM TO THE ABOVE ADDRESS.

1. REPORT DATE *(DD-MM-YYYY)*	2. REPORT TYPE	3. DATES COVERED *(From - To)*

4. TITLE AND SUBTITLE	5a. CONTRACT NUMBER
	5b. GRANT NUMBER
	5c. PROGRAM ELEMENT NUMBER
6. AUTHOR(S)	5d. PROJECT NUMBER
	5e. TASK NUMBER
	5f. WORK UNIT NUMBER

7. PERFORMING ORGANIZATION NAME(S) AND ADDRESS(ES)	8. PERFORMING ORGANIZATION REPORT NUMBER

9. SPONSORING/MONITORING AGENCY NAME(S) AND ADDRESS(ES)	10. SPONSOR/MONITOR'S ACRONYM(S)
	11. SPONSOR/MONITOR'S REPORT NUMBER(S)

12. DISTRIBUTION/AVAILABILITY STATEMENT

13. SUPPLEMENTARY NOTES

14. ABSTRACT

15. SUBJECT TERMS

16. SECURITY CLASSIFICATION OF:			17. LIMITATION OF ABSTRACT	18. NUMBER OF PAGES	19a. NAME OF RESPONSIBLE PERSON
a. REPORT	b. ABSTRACT	c. THIS PAGE			
					19b. TELEPHONE NUMBER *(Include area code)*

AN INVESTIGATION OF A DYNAMIC SENSOR MOTION STRATEGY

Nathan P. Yerrick

Air Force Research Laboratory, Munitions Directorate
Eglin AFB, FL
nathan.yerrick@eglin.af.mil

Abhishek Tiwari

Engineering and Applied Sciences, California Institute of Technology
Pasadena, CA
atiwari@cds.caltech.edu

David E. Jeffcoat

Air Force Research Laboratory, Munitions Directorate
Eglin AFB, FL
david.jeffcoat@eglin.af.mil

This paper considers a dynamic sensor coverage problem in which a single mobile sensor attempts to monitor multiple sites. Sensor motion is modeled using a discrete time, discrete state Markov process. State dynamics at each site are modeled as a linear system. A stochastic simulation is used to demonstrate previously derived theoretical conditions under which a single sensor is or is not sufficient to maintain a bounded estimate of the state of every site. Observations are made about the relationship of sensor motion to system dynamics. A strategy is presented to find a good sensor motion model based upon the system dynamics and to determine the convexity of the solution set.

1. Introduction

"Sensor coverage is the problem of deploying multiple sensors in an unknown environment for the purpose of automatic surveillance, cooperative exploration or target detection [5]." Sensors can either cover an area of interest statically (fixed sensors) or dynamically (mobile sensors). Static coverage can be used when the area or objects of interest can be completely covered by the associated sensors. However, dynamic coverage becomes necessary when the available sensors cannot adequately cover the area or objects of interest from fixed positions.

2. Problem Description

This chapter focuses on the dynamic sensor coverage problem when there is only one sensor available to cover N sites. This research is an extension of the work accomplished by Tiwari, *et al.* in [5]. Each site is defined to be a discrete time linear system located at a unique point in space. The sensor maintains discrete time Kalman filter estimates of an attribute of interest at each site, but is constrained to only measuring the attribute of the site where it is physically located at a given instant in time. An indicator function, described by Sinopoli in [4], ensures that if the sensor is over site i at time k, both the measurement and time updates of the Kalman filter are executed for site i. However, if the sensor is not over site i at time k, then only the time update is executed for site i.

The physical realization of this problem could range from estimating the changing temperature in several buildings to estimating the pollution emission levels of several manufacturing plants in an area. In these examples, the attributes would be temperature and pollution emissions, respectively. The changing attributes of each site are modeled in the following manner. Consider N independently evolving linear time invariant (LTI) systems, whose dynamics are given by

$$
\begin{aligned}
x_{k+1} &= Ax_k + w_k \\
y_k &= Cx_k + v_k
\end{aligned}
\tag{1}
$$

where x_k, x_{k+1}, $w_k \in \mathbb{R}^{n \times 1}$ and y_k, $v_k \in \mathbb{R}^{m \times 1}$, w and v are Gaussian random vectors with zero mean and covariance matrices Q and R respectively. In this chapter, we track only one attribute per site. Since all sites' attributes are independent, the information pertaining to the attribute is found on the diagonals of A, C, Q, and R. For instance, all information regarding the attribute at site two would be contained at A_{22}, C_{22}, Q_{22}, and R_{22}.

The goal of the Kalman filter is to keep a bounded estimate of the *a priori* error covariance between the random vectors x_k and $\hat{x}_k$; that is, the true state of the system and the estimate of the system state at time k, respectively. The *a priori* error covariance, i.e. the error covariance on the 'time update' side of the Kalman filter, at time k and location i is denoted $P_{i,k}^-$ and is defined as

$$P_{i,k}^- = E[(x_k - \hat{x}_k^-)(x_k - \hat{x}_k^-)^\mathrm{T}].\tag{2}$$

In general, the dynamic coverage problem is said to have been solved, if for N sites, the limit of the expected value of the error covariance as k approaches infinity is finite for all sites, if $P_{i,0}^- \geq 0$. Similarly, if the limit of the expected value of the error covariance as k approaches infinity is unbounded for some $P_{i,0}^- \geq 0$, then the dynamic coverage problem is not solved. If the error covariance is unbounded at any site, the system is referred to as unstable; if the system is bounded for all sites, it is referred to as stable [6].

The sensor's motion can be modeled as an independently and identically distributed (IID) random process or by a discrete time discrete state (DTDS) ergodic Markov chain. This chapter only considers the Markov chain model. The concept of steady state ergodic Markov chains is described in depth in [2] and [3]. For simplicity, we assume that the sensor can move instantaneously from one site to another at any time k. The DTDS Markov chain has a transition probability matrix T, where T_{ij} is the probability that the sensor will be at site j at time $k+1$ given that the sensor was at site i at time k. T_{ii}, the ith diagonal entry of the transition probability matrix, denotes the probability that the sensor remains at site i at time $k+1$ given that the sensor was at site i at time k. Also, let π_i be the steady state probability of finding the sensor at site i.

The conditions under which the coverage problem is or is not solved were already discussed in a qualitative sense; now those conditions will be explicitly defined for sensor motion described by an ergodic Markov chain.

(a) Let (A, C) be detectable and $(A, \sqrt{Q})$ be observable, then the sensor fails to solve the coverage problem if at least one of the following conditions hold:

$$\frac{1-\pi_i(2-T_{ii})}{1-\pi_i} > \frac{1}{\alpha_i^2}, \quad i \in 1,2,...,N \tag{3}$$

where α_i is the eigenvalue of A associated with site i. Note: in this chapter, since every site is independent, all off-diagonal elements will be zero, so α_i will simply be the value of A_{ii} [5].

(b) If matrix C is invertible, then the sensor solves the coverage problem if all of the following conditions hold [5]:

$$\frac{1-\pi_i(2-T_{ii})}{1-\pi_i} < \frac{1}{\alpha_i^2}, \quad i \in 1,2,...,N. \tag{4}$$

If the coverage problem is solved, then a lower and upper bound of the expected value of the error covariance, $E[P_{i,k}^-]$, can be obtained based on π_i, T_{ii}, A, C, Q, R, and $P_{i,0}$. Reference [5] provides additional detail on these bounds. If the bounds diverge for at least one site, then the coverage problem is not solved. However, if the bounds converge for all sites, then the coverage problem is solved. Equations (4) and (5) will later be referred to as feasibility inequalities. Figures 1(a) and 1(b) illustrate bounds for both stable and unstable sites.
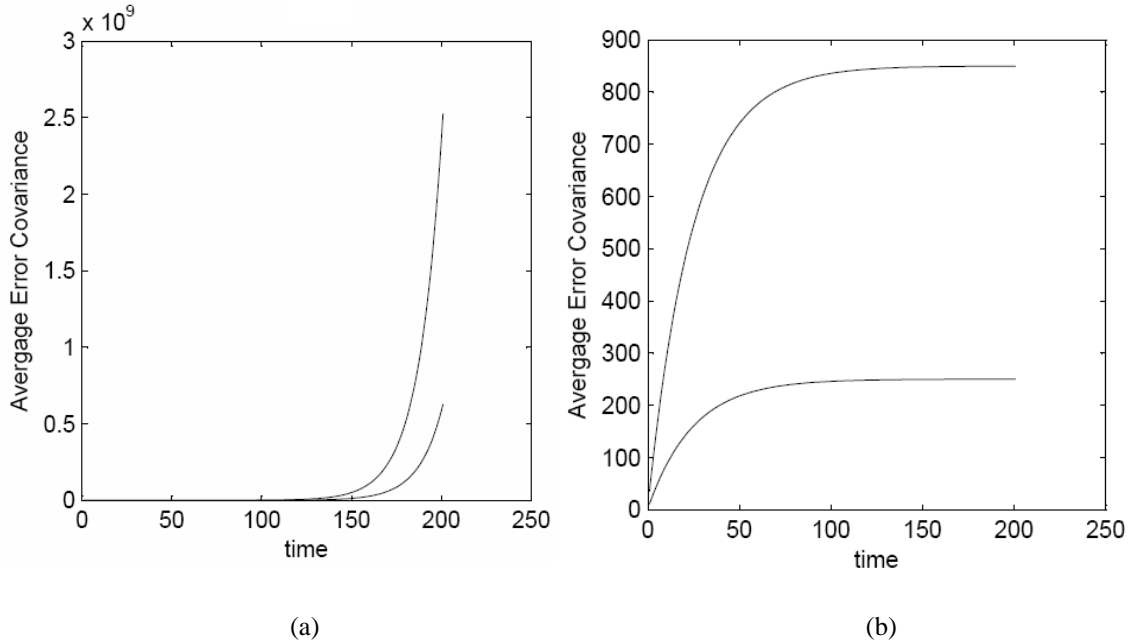
Fig. 1. Figure (a) shows a typical unstable site: both bounds diverge. Figure (b) shows a stable site: both bounds converge.

3. Simulation: Checking the Theory

3.1 Simulation Approach

Intuition suggests that the faster the system dynamics of a site relative to other sites, the more time the sensor must spend over this site. Also, it makes sense that the sensor must divide its attention among the sites according to the dynamics of the attribute of each site. The theory in [5] confirms this intuition. We now provide a simulation both to demonstrate the theory and to provide additional insights into the relationship between sensor motion and the dynamics of each site.

A Monte Carlo simulation was built in MATLAB$^{®}$ using a DTDS Kalman filter with an indicator function and a DTDS Markov chain. The error covariance was computed at each site for all time iterations over multiple replications. The average error covariance over the multiple replications was calculated for all time iterations and plotted with the appropriate error covariance bounds for each site. The values used for equation (1) in the simulation were $C_{ii} = 0.2$, $Q_{ii} = 10$, and $R_{ii} = 2$ for all sites.

The feasibility inequalities in equations (4) and (5) not only convey whether or not the coverage problem is solved, but also indicate, given the dynamics of each site, whether or not a given transition probability matrix provides a feasible solution to the problem. Refer to Figure 2 for the following discussion. As discussed in the Section 2, if at least one site's bounds are divergent; i.e., if the feasibility inequality in equation (4) is not satisfied for at least one site, then the transition probability matrix does not provide a feasible solution to the coverage problem. Note that the bounds in Figure 2(c) are divergent and that the inequality in Figure 2(f) is not satisfied. However, in Figures 2(d) and

2(e), the bounds are convergent, indicating that both inequalities in Figures 2(g) and 2(h) are satisfied. In this case, the overall coverage problem is not solved because the dynamics at site one cannot be adequately monitored.
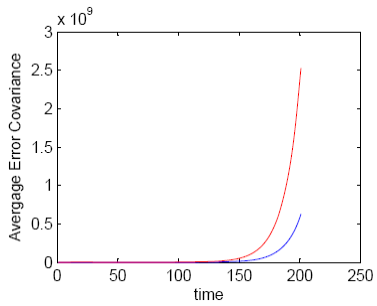
$$A = \begin{bmatrix} 1.3 & 0 & 0 \\ 0 & 1.2 & 0 \\ 0 & 0 & 1.1 \end{bmatrix}$$
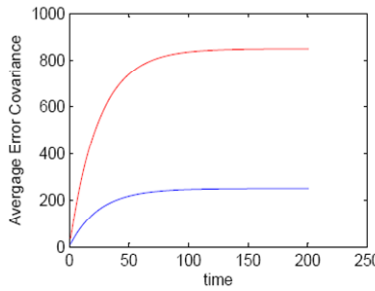
(a) System Dynamics

$$T = \begin{bmatrix} .36111 & .33333 & .30556 \\ .36111 & .33333 & .30556 \\ .36111 & .33333 & .30556 \end{bmatrix}$$
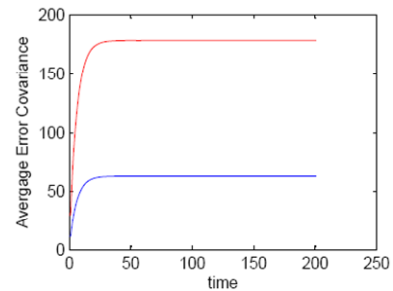
$$\pi = [0.36111, 0.33333, 0.30556]$$

(b) Sensor Motion

(c) Bounds for Site 1

(d) Bounds for Site 2

(e) Bounds for Site 3

$$\frac{1 - .36111\,(2 - .36111)}{1 - .36111} > \frac{1}{1.3^2}$$

$$.63889 > .59172$$

(f) Inequality for Site 1

$$\frac{1 - .33333\,(2 - .33333)}{1 - .33333} < \frac{1}{1.2^2}$$

$$.66667 < .69444$$

(g) Inequality for Site 2

$$\frac{1 - .30556\,(2 - .30556)}{1 - .30556} < \frac{1}{1.1^2}$$

$$.69444 < .82644$$

(h) Inequality for Site 3

Fig. 2. This figure shows that the bounds computed in simulation match the feasibility inequalities. The feasibility inequality at site 1 is not satisfied, and the bounds at site 1 are divergent. The feasibility inequalities at site 2 and 3 are satisfied, indicating that the bounds at sites 2 and 3 converge.

3.2 Simulation Observations

3.2.1 Case I: System Dynamics Equal, Transition Probabilities Varied

Next, we examine a case in which the system dynamics are the same across all sites. The transition probability matrix is constructed so that the coverage problem is solved, even though each site receives a different amount of "sensor attention." In this case, site one will be visited by the sensor most often, and site three will be visited least

often [Figure 3]. Each dot in Fig. 3 represents the average error covariance over 10,000 Monte Carlo replications. There are 200 dots at each site, one for each time step. As a site gets less sensor attention, we notice several effects: the bounds converge more slowly, the scale of the bounds is increased, and more dots are outside of the bounds. As a site nears the point of instability, the bounds begin to look more like a line than a curve.
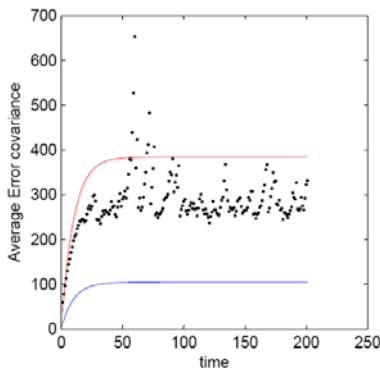
$$A = \begin{bmatrix} 1.2 & 0 & 0 \\ 0 & 1.2 & 0 \\ 0 & 0 & 1.2 \end{bmatrix}$$

$$T = \begin{bmatrix} .372 & .32 & .308 \\ .372 & .32 & .308 \\ .372 & .32 & .308 \end{bmatrix}$$
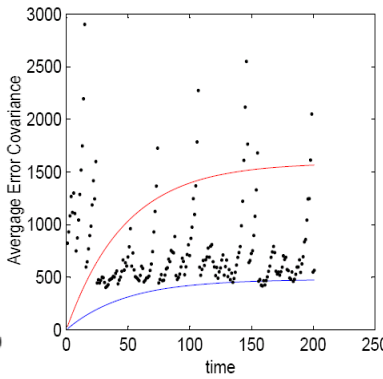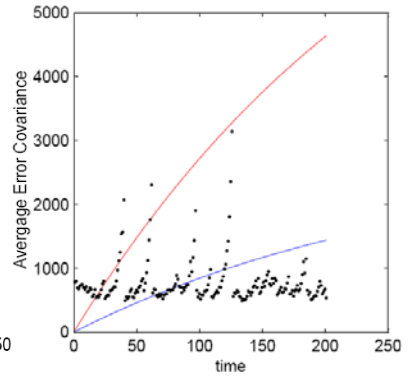
$$\pi = [0.372, 0.32, 0.308]$$

(a) System Dynamics   **(b) Sensor Motion**

(c) Site 1   **(d) Site 2**   **(e) Site 3**

Fig. 3. This figure shows Monte Carlo simulation trends when the system dynamics are equal at each site and the sensor motion is varied.

3.2.2 Case II: System Dynamics Varied, Transition Probabilities Equal

In this case, the transition probability matrix is approximately equal for all sites, meaning that every site will be visited approximately the same number of times. The system dynamics vary across the three sites: site one has the fastest dynamics and site three has the slowest dynamics [Figure 4]. The varied dynamics cause results similar to the varied sensor attention in the last scenario. As a site's dynamics get slower, the bounds' scales decrease, the number of dots outside the bounds decrease, and the time required for the bounds to converge gets smaller. Also, as can be seen in Figure 4(e), when a site's dynamics are slow, and it receives sufficient attention from the sensor, the sample error covariances tend to form a horizontal line well within the bounds.
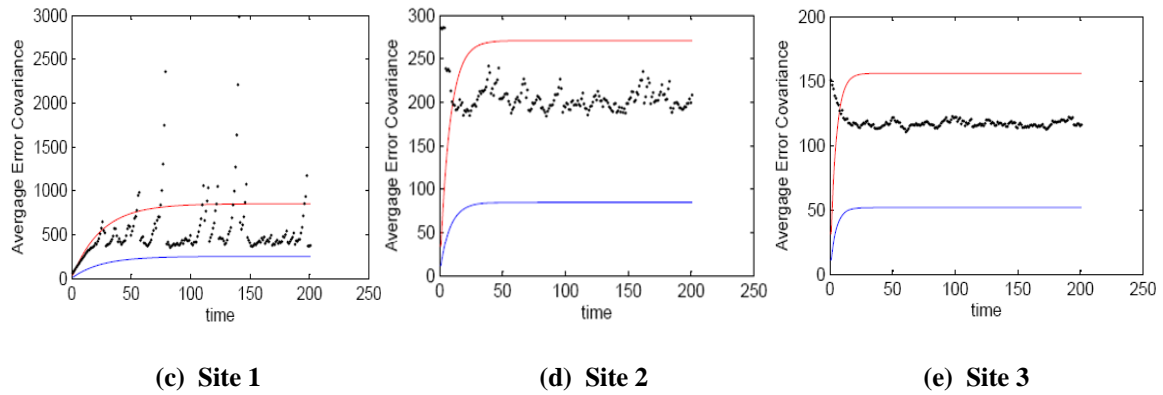
$$A = \begin{bmatrix} 1.2 & 0 & 0 \\ 0 & 1.15 & 0 \\ 0 & 0 & 1.1 \end{bmatrix} \qquad T = \begin{bmatrix} .3334 & .3333 & .3333 \\ .3333 & .3334 & .3333 \\ .3333 & .3333 & .3334 \end{bmatrix}$$

$$\pi = [0.3333, 0.3333, 0.3333]$$

(a) System Dynamics **(b) Sensor Motion**

(c) Site 1 **(d) Site 2** **(e) Site 3**

Fig. 4. This figure shows Monte Carlo simulation trends when the system dynamics are varied at each site and the sensor motion is equal for all sites.

3.2.3 Summary of Observations

The Monte Carlo simulations confirm both theory and intuition. It is clear in the simulation results that as a site gets more sensor attention, the average error covariance is more likely to cluster within the bounds. We also note that the slower the dynamics of a site, the less sensor attention is needed to ensure that the error covariance remains bounded and stable. Finally, when a slowly evolving site has sufficient sensor attention, the average error covariance remains well within the bounds.

In the next section, we introduce a method that exploits the system dynamics to find a good, although not necessarily optimal, sensor motion model.

4. Optimization: Finding a good sensor motion model given the system dynamics

4.1 Optimization Approach

In this section, we present an approach to determine a good transition probability matrix given a model of site dynamics. Note that the existence of a method that guarantees an optimal solution remains an open question.

The approach presented in this section is a genetic-based heuristic algorithm called scatter search implemented in MATLAB®. The goal of this meta-heuristic is to provide both intensification and diversification of the solution: intensification meaning that the algorithm uses randomly created feasible solutions to progressively find better

results with respect to the objective function, and diversification meaning that the algorithm uses differences between randomly created feasible solutions to increase the chances of finding the best solution available.

The objective function is based on the feasibility inequalities discussed earlier. The objective is to minimize the maximum ratio over all N sites, as shown in (5), subject to typical probability constraints on π and on the rows of T.

$$\min\left\{\max_{i\in[1,2,\ldots,N]}\left(\frac{\dfrac{1-\pi_i(2-T_{ii})}{1-\pi_i}}{\dfrac{1}{\alpha_i^2}}\right)\right\} \tag{5}$$

This min/max objective will be referred to as the performance indicator; the smaller the performance indicator, the better the solution.

In general, the algorithm performs the following process. First, initial solutions for T are randomly generated. A solution is retained if it is determined to be feasible based on equation (4). Next, linear combinations of feasible solutions are constructed to form new solutions. Each solution is assigned a score based upon the objective function (5), and each solution is ranked according to its score. After a set number of iterations in which no better score is obtained, the algorithm is terminated. The solution with the lowest performance indicator is presented as the best solution found.

The simulation was also used to investigate whether the set of feasible solutions is convex. First, solutions were constructed so that the solutions were feasible, but very close to the infeasibility boundary. Next, linear combinations of these close-to-the-boundary solutions were formed, using equation (6), with $\lambda \in [0,1]$. If any linear combination of two initial solutions was found to be infeasible, then the solution set cannot be convex. In fact, more than one infeasible solution was found, so the solution set of all feasible solutions is not convex by demonstration. The matrices shown in Figure 5 show one example where the linear combination of two feasible solutions formed an infeasible solution. In this example, $\lambda = 0.5$, the system dynamics are shown in Figure 5(a), and T_1 and T_2 represent the two feasible solutions in Figures 5(b) and 5(c).

$$T_3 = \lambda T_1 + (1-\lambda)T_2 \tag{6}$$

$$A = \begin{bmatrix} 1.3 & 0 & 0 \\ 0 & 1.2 & 0 \\ 0 & 0 & 1.1 \end{bmatrix}$$

(a)

$$T_1 = \begin{bmatrix} 0.63105 & 0.3185 & 0.050452 \\ 0.37456 & 0.20869 & 0.41675 \\ 0.46796 & 0.27469 & 0.25734 \end{bmatrix} \qquad T_2 = \begin{bmatrix} 0.32893 & 0.27175 & 0.39932 \\ 0.46596 & 0.53137 & 0.0026781 \\ 0.29887 & 0.41671 & 0.28442 \end{bmatrix}$$

(b)   (c)

Fig. 5.

4.2 Optimization Results

This section presents results of the optimization algorithm. The effectiveness of the heuristic is demonstrated by comparing solutions generated by the algorithm with randomly generated feasible solutions. Feasible solutions are generated by creating random transition probability matrices constrained so that each row sum is one. The equilibrium probability vector, π_i, is computed for each matrix, then the feasibility inequalities are checked. Those transition matrices that provide a feasible solution are saved. Heuristic solutions are compared to random feasible solutions under two cases that differ in the underlying site dynamics.

4.2.1 Case I: Faster Dynamics

For the first case, one hundred feasible solutions were randomly created with site dynamics modeled by matrix A in Figure 6(a). The mean of the performance indicators from the 100 random solutions was 0.9729, the sample standard deviation was 0.0246, and the minimum and maximum values were 0.9010 and .9997, respectively. The heuristic solution had a performance indicator of 0.8901, a 9% improvement. Figures 6 and 7 show a graphical representation of a randomly created solution and a heuristic solution, respectively. The main difference between the figures is the scale of the bounds. Also, there are more dots outside the bounds in Figure 6 than in Figure 7.
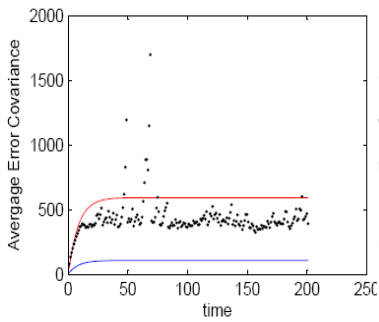
$$A = \begin{bmatrix} 1.35 & 0 & 0 \\ 0 & 1.3 & 0 \\ 0 & 0 & 1.25 \end{bmatrix}$$

$$T = \begin{bmatrix} .22925 & .41638 & .35437 \\ .53443 & .060045 & .405525 \\ .49143 & .44609 & .06248 \end{bmatrix}$$
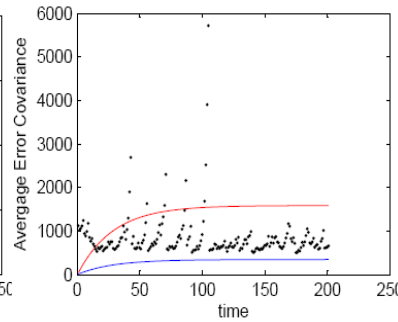
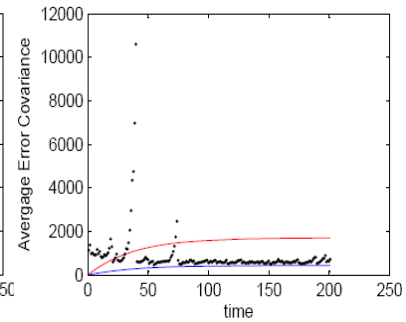$$\pi = [0.40002, 0.31327, 0.28671]$$

(a) System Dynamics

(b) Sensor Motion

(c) Site 1

(d) Site 2

(e) Site 3

Fig. 6. This figure shows the graphical depiction of a representative randomly created solution with a performance indicator of 0.9737.
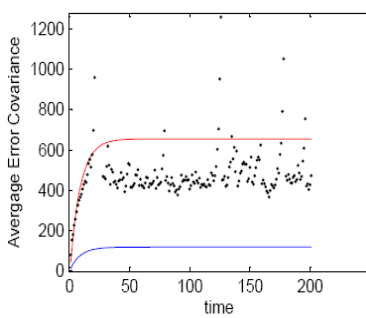
$$A = \begin{bmatrix} 1.35 & 0 & 0 \\ 0 & 1.3 & 0 \\ 0 & 0 & 1.25 \end{bmatrix}$$

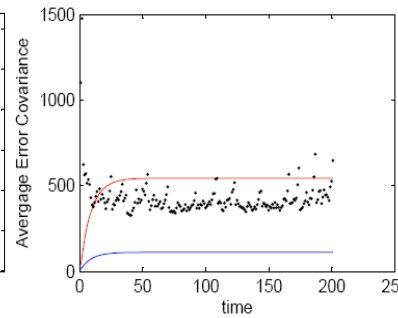$$T = \begin{bmatrix} .02626 & .47878 & .49476 \\ .53819 & .09512 & .36669 \\ .48273 & .46732 & .04995 \end{bmatrix}$$
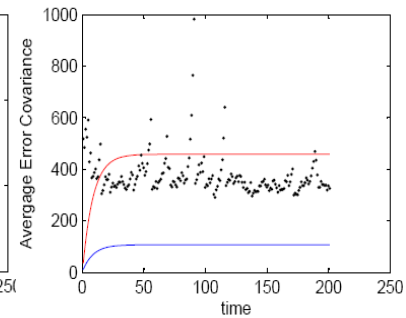
$$\pi = [0.34456, 0.34344, 0.312]$$

(a) System Dynamics

(b) Sensor Motion

(c) Site 1

(d) Site 2

(e) Site 3

Fig. 7. This figure shows the heuristic solution in graphical form for the case of faster dynamics. The performance indicator in this case is 0.89007.

4.2.2 Case II: Slower Dynamics

In the second comparison, one hundred feasible solutions were randomly created with slower dynamics, modeled by Figure 8(a). The mean of the performance indicators from the 100 random solutions was 0.9398, the sample standard deviation was 0.0469, and the minimum and maximum values were 0.7624 and 0.9991, respectively. The heuristic solution had a performance indicator of 0.7027, a 25.2% improvement. From the two comparison scenarios representing faster and slower dynamics, we note that the heuristic's performance is better when the dynamics are slower. Figures 8 and 9 depict a randomly created solution and a heuristic solution, respectively, for the case of slower dynamics. In both figures, the error covariances tend to form a straight line within the bounds. The main difference between the figures is in the mean of the average error covariances. Also, the magnitude of the bounds in Figures 9(c), 9(d), and 9(e) is consistently less than in Figures 8(c), 8(d), and 8(e).

One observation from Figure 9(b) is counter-intuitive. We would expect a site with faster dynamics to warrant more sensor attention than sites with slower dynamics, but the heuristic solution in this case does not bear this out. We note that π_3 is greater than π_1 and π_2, even though site three has the slowest dynamics [Figure 9(b)]. Intuition would suggest that π_3 should be the smallest steady-state probability.

$$A = \begin{bmatrix} 1.2 & 0 & 0 \\ 0 & 1.15 & 0 \\ 0 & 0 & 1.1 \end{bmatrix}$$

$$T = \begin{bmatrix} .359696 & .51803 & .12228 \\ .09796 & 0.50007 & .40197 \\ .80044 & .12095 & .07861 \end{bmatrix}$$

$$\pi = [0.3511, 0.41935, 0.22954]$$

(a) System Dynamics

(b) Sensor Motion
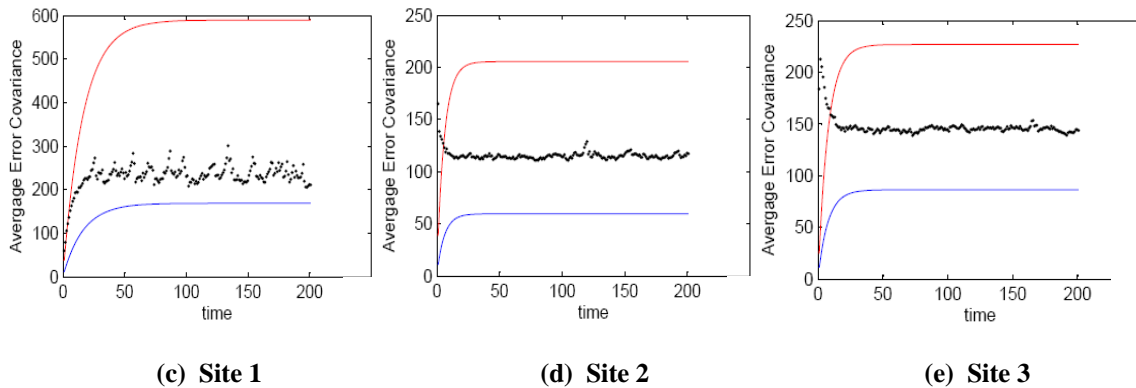
(c) Site 1

(d) Site 2

(e) Site 3

Fig. 8. This figure shows the graphical depiction of a representative randomly created solution that has a performance indicator of 0.9411.

$$A = \begin{bmatrix} 1.2 & 0 & 0 \\ 0 & 1.15 & 0 \\ 0 & 0 & 1.1 \end{bmatrix}$$

$$T = \begin{bmatrix} 0 & .5004 & .4996 \\ .6649 & 0 & .3351 \\ .3706 & .4372 & .1922 \end{bmatrix}$$
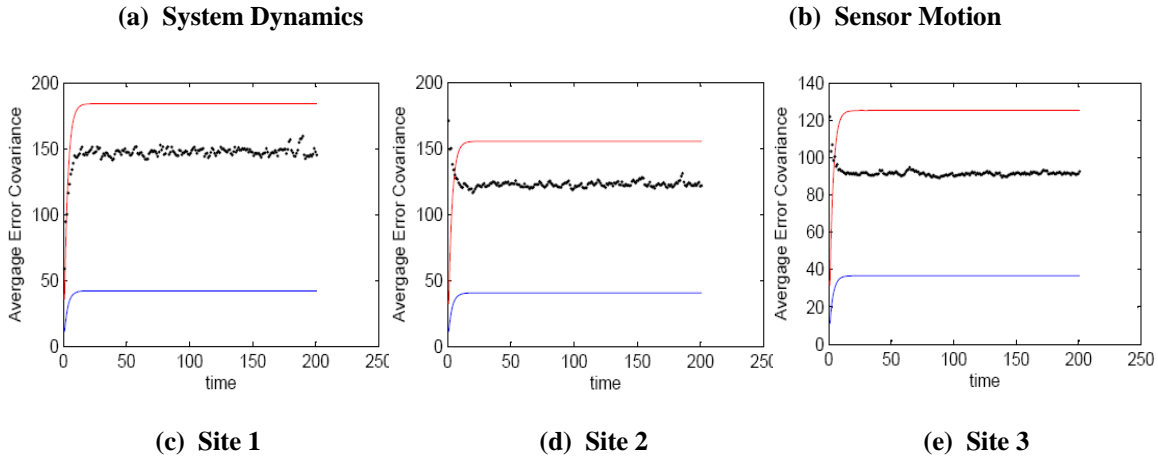
$$\pi = [0.33891, 0.31911, 0.34198]$$

(a) System Dynamics

(b) Sensor Motion

(c) Site 1

(d) Site 2

(e) Site 3

Fig. 9. This figure shows the heuristic solution in graphical form for the case of slower dynamics. The performance indicator was 0.7027.

5. Summary and Future Work

The goal of this chapter was to demonstrate the theory of the dynamic sensor coverage problem in the case of a single sensor whose motion is modeled by a DTDS Markov chain. The Monte Carlo simulation demonstrated that the theory developed in [5] matched both intuition and empirical results. Another goal was to show that an improved transition probability matrix can be found using a heuristic. An improvement over random feasible solutions was found using scatter search, though this method does not guarantee a global optimum. The search did provide solutions that were sometimes counter-intuitive. The heuristic performed best in cases with relatively slower system dynamics. The algorithm run time depends on the exact conditions specified, but for the conditions specified in this research, the optimization algorithm required from two to four minutes of run time on a desktop PC. We also showed by demonstration that the set of feasible solutions is not convex.

Future work will include refined optimization approaches for the single sensor case and extensions to multiple sensors. For the single sensor, an effort will be made to understand why the heuristic produces results that are counter-intuitive with respect to the division of sensor attention, and to further explore under what conditions the scatter search heuristic performs best. The heuristic will also be used to provide insights that might lead to a theoretical solution to the problem of determining an optimal transition matrix.

Acknowledgments

References

[1] Brown, Robert G., and Patrick Hwang. *Introduction to Random Signals and Applied Kalman Filtering*. 2nd ed. New York: John Wiley & Sons, Inc., 1992. 231-240.

[2] Fisz, Marek. *Probability Theory and Mathematical Statistics*. 3rd ed. New York: John Wiley & Sons, Inc., 1963. 271-325.

[3] Kleinrock, Leonard. *Queueing Systems*. Vol. 1. New York: John Wiley & Sons, Inc., 1975. 30-52.

[4] Sinopoli, Bruno, Luca Schenato, Massimo Franceschetti, Kameshwar Poolla, Michael I. Jordan, and Shankar S. Sastry. "Kalman Filtering with Intermittent Observations." *IEEE Transactions on Automatic Control,* vol. 49, no. 9, pp. 1453-1464, Sept. 2004.

[5] Tiwari, A., M. Jun, D. Jeffcoat, and R. Murray, "The Dynamic Sensor Coverage Problem," *16th International Federation of Automatic Control (IFAC) World Congress*, Prague, Czech Republic, July 2005

[6] Welch, Greg, and Gary Bishop. *An Introduction to the Kalman Filter*. Univ. of North Carolina at Chapel Hill, 2004.